

WALL SHEAR STRESS MEASUREMENT OF NEAR-WALL FLOW OVER INCLINED AND CURVED BOUNDARIES

Thien Duy Nguyen, John Craig Wells

Department of Civil Engineering
Ritsumeikan University
1-1-1 Noji Higashi, Kusatsu, Shiga, 525-8577, Japan
gr044050@se.ritsumei.ac.jp, jwells@se.ritsumei.ac.jp

Chuong Vinh Nguyen

Department of Mechanical Engineering
Monash University
VIC 3800, Australia
Chuong.Nguyen@eng.monash.edu.au

ABSTRACT

In investigations of near-wall turbulent flow, wall shear measurement is often important. Particle Image Velocimetry (PIV) technique is now the predominant measurement tool in experimental fluid mechanics. Nevertheless, conventional PIV is restricted in very near walls. This paper proposes a near-wall measurement technique, named Interfacial PIV (IPIV), that extends our recent works on PIV, called “Interface Gradiometry” (Nguyen and Wells, 2004, 2006). Interfacial PIV deals with curved boundaries by means of conformal transformation, allows us to directly measure the wall shear gradient, and yields a near-wall tangential velocity profile at one pixel resolution. In IPIV, we propose an algorithm of wall-normal integration of measured velocity gradient, an approach with built-in validation capability that overcomes the limitations of conventional PIV processing techniques in near-wall flow measurement. It is feasible to apply IPIV to Stereo PIV images to measure wall gradients by stereo reconstruction. In this paper, wall gradients (with and without stereo reconstruction) and tangential velocity profiles by IPIV to synthetic images of turbulent flow over a wavy bed are compared to those by Particle Image Distortion (Huang et al, 1993) and benchmarked with DNS data. In addition, experiments on turbulent open channel flow over a backward-facing step (BFS) with multiple synchronized PIV cameras are presented with results from IPIV to 2C and Stereo experimental images.

INTRODUCTION

The important roles of wall shear gradients and/or near-wall flows in turbulence have brought many interested questions to researchers. However, standard PIV is ill-suited to near-wall flow because of low seeding density, high velocity gradient and strong wall reflections. It requires much prudence to either reduce the spurious velocity vectors if the PIV interrogation window partly includes the boundary or deform/ rotate the interrogation window appropriating to each segment of wall. Such problems are aggravated if standard PIV is performed next to curved boundaries which are commonly found in many industrial and medical applications.

To mitigate the problems of conventional PIV in high shear regions, Huang et al. (1993) proposed Particle Image Distortion (PID). This method distorts a particle image according to velocity field initially measured by standard cross-correlation PIV to iteratively compensate the estimated deformation.

To improve the accuracy of PIV measurements in interrogation windows that partly include the non-fluid region or wall boundary, Hochareon et al. (2004) re-located detected displacement vectors to the centroid of the fluid region.

Nguyen and Wells (2004) proposed “PIV/ Interface Gradiometry (PIV/IG) to directly measure the velocity gradients by shearing the PIV image templates parallel to a no-slip wall, and to perform stereo-reconstruction of wall shear gradients as well. The stereo reconstruction of wall gradients are noted in equ. 1, wherein (x, y, z) and (X, Y) denote the physical and pixel coordinates respectively. Superscripts (1), (2) are camera numbers used in the Stereo PIV system. The equation of stereo reconstruction of gradients has the same form as that of velocity reconstruction, and can be solved analogously by least squares for the unknowns $\frac{\partial u}{\partial y}$ and $\frac{\partial w}{\partial y}$. Superior to differentiation of conventional PIV data for measuring wall shear gradient, PIV/IG was however limited to straight walls aligned with the array sensor’s pixel.

$$\begin{bmatrix} \frac{\partial U^{(1)}}{\partial y} \\ \frac{\partial V^{(1)}}{\partial y} \\ \frac{\partial U^{(2)}}{\partial y} \\ \frac{\partial V^{(2)}}{\partial y} \end{bmatrix} = \begin{bmatrix} \frac{\partial X^{(1)}}{\partial x} & \frac{\partial X^{(1)}}{\partial y} & \frac{\partial X^{(1)}}{\partial z} \\ \frac{\partial X^{(2)}}{\partial x} & \frac{\partial X^{(2)}}{\partial y} & \frac{\partial X^{(2)}}{\partial z} \\ \frac{\partial Y^{(1)}}{\partial x} & \frac{\partial Y^{(1)}}{\partial y} & \frac{\partial Y^{(1)}}{\partial z} \\ \frac{\partial Y^{(2)}}{\partial x} & \frac{\partial Y^{(2)}}{\partial y} & \frac{\partial Y^{(2)}}{\partial z} \end{bmatrix} \begin{bmatrix} \frac{\partial u}{\partial y} \\ \frac{\partial v}{\partial y} \\ \frac{\partial w}{\partial y} \end{bmatrix} \quad (1)$$

To deal with curved boundaries and very near-wall flows, Nguyen and Wells (2006) proposed some extensions of PIV/IG, denoted as PIV/IG+. It consisted of a conformal transformation technique to stretch image segments above a curved wall to rectangles, and a novel 1D correlation function to produce a “correlation stack” that contains the tracer’s tangential displacement in wall-normal direction.

Recently, we have achieved some advances of PIV/IG+, hereinafter named as Interfacial PIV (IPIV). With IPIV, we have succeeded in testing with 2D synthetic images and validated with DNS data (Nguyen et al. 2008). This paper will briefly describe 3 benefits of IPIV as: (i) the image transformation, (ii) the novel technique to directly measure the wall shear gradient and (iii) precisely extract the tangential velocity profile from the correlation stack. In addition, utilization of IPIV in wall shear measurements to 3D synthetic images from a DNS snapshot of a turbulent flow over a wavy bed is also mentioned in details. Corresponding results will be compared with those resulted from PID and IPIV to 2D image pairs. All obtained wall shear gradients are benchmarked with the true DNS values.

Moreover, open flume tests with a backward-facing step (BFS) at a low-Reynolds number $Re_h = 2200$, based on step height h and mean streamwise velocity U_0 , were introduced. A system of a two-component (2C) PIV linked with a Stereo PIV was conducted to examine the flow structure behind the step. Applications of IPIV to 2CPIV and Stereo PIV experimental images were employed. The obtained wall

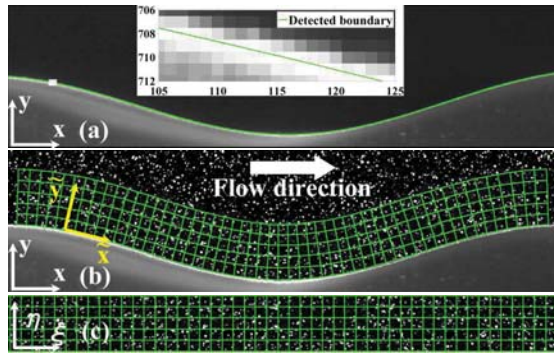


Figure 1: Wall detection and image transformation to deal with a curved boundary. (a) Detected boundary by Laplacian of Gaussian method, (b) Generated orthogonal, curvilinear grids shown only 1 for 20 grid lines, (c) transformed near-wall image by 2D interpolation.

shear gradients then were used to determine the mean reattachment length with high resolution towards the wall.

INTERFACIAL PIV

A review of Interfacial PIV is presented here. Building on our previous work (Nguyen and Wells, 2006), IPIV procedure consisted of 5 steps:

- Identifying wall boundary
- Conformally transforming near-wall image region to rectangle
- Calculating line-correlation to produce correlation stack
- Measuring wall shear gradient and integrating tangential velocity
- Reverse transforming to obtain physical values.

Within this recipe, steps 2 and 5 introduced a new proposal for near-wall PIV, and can be applied independently of others, i.e. can be followed by any suitable PIV processing techniques.

Identifying wall boundary

The accuracy of wall identification strongly affects the accuracy of Interfacial PIV technique when the boundary condition is assumed to be no-slip (Nguyen et al, 2006b). Based on our experience so far, a second-order edge detection algorithm by Marr and Hildreth (1980), named Laplacian of Gaussian, seems to be the most appropriate with our experimental images, in which strong wall reflection is observed. In this paper, we assumed that the boundary is fixed. Then the accuracy of wall detection is clearly improved after noise suppressing by sample averaging of images. The averaged image is convolved with a Gaussian kernel for smoothing before being applied to a second-order operator. From the resulting image, raw wall positions are detected by searching zero-crossing points, then smoothed by low-pass filtering with a Fourier kernel. Fig. 1a exemplifies the detected boundary from experimental images of a water channel with a sinusoidal wall.

Conformally transforming near-wall image region to rectangle

Next, an orthogonal curvilinear grid whose lower boundary lies on the detected wall is generated (cf. fig. 1b). A

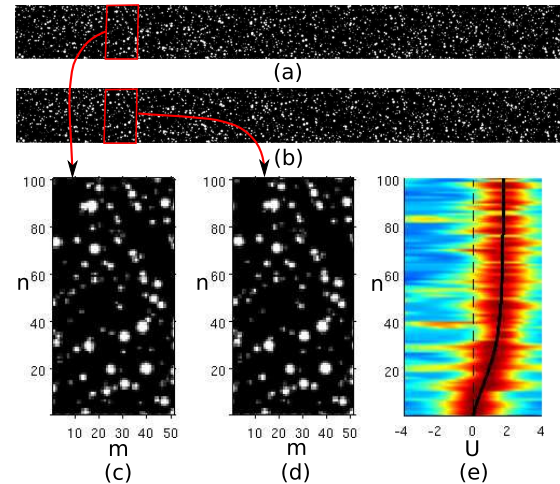


Figure 2: Line correlation applied to templates (c), (d) of transformed images (a), (b) yielding normalized correlation stack (e), black dashed curve is DNS profile

curved image segment in physical domain (x, y) is then conformally transformed into a rectangle, named transformed domain (ξ, η) . The image intensities of the transformed template are produced by bicubic interpolation from corresponding intensities inside the grid region (cf. fig. 1c). The orthogonality of the grids is preserved by conformal mapping function (Ives and Zacharias, 1987).

In near-wall measurements, a local coordinate system (\tilde{x}, \tilde{y}) aligned to wall surface is often used to express local wall flow properties, such as wall shear gradient and near-wall velocity profile. The local coordinate system, however, varies along the curved wall, and we find it easier to obtain the local flow properties by computing them from the transformed domain and then reverse transforming back to the physical domain.

Benefits of our conformal transformation can be reviewed in Nguyen et al. (2008), in which, wall shear gradients by PID applied to rectangle transformed images showed better agreement to DNS data than those by standard PIV with centroid shifting correction applied to non-transformed images.

Calculating stack of line correlation

As designed to deal with near-wall flows, IPIV requires that the wall-normal interframe tracer displacement be less than particle image diameter. If this condition is satisfied, a purely tangential search can produce a correlation peak. In this scene, we propose a 1D correlation function, named line correlation, to produce a “stack” of 1D correlation curves. The correlation coefficient $C_{U,n}$ is calculated by cross-correlating the intensity distribution $I(m)$ along each line n on the template of the first exposure with the corresponding pixel line on the template of the second exposure:

$$C_{U,n} = \sum_{m=1}^M (I_{m+U,n} - \bar{I}_{U,n})(I'_{m,n} - \bar{I}'_n) \quad (2)$$

(M, N) are the width and height, and (m, n) are the pixel coordinates of a template in rectangular transformed image. $\bar{I}_{U,n}$ and \bar{I}'_n are the mean intensities on each pixel line of the first and second templates. U is the displacement coordinate in the resulting correlation stack. The correlation coefficient $C_{U,n}$ normalized with r.m.s of $(I_{m+U,n} - \bar{I}_{U,n})$

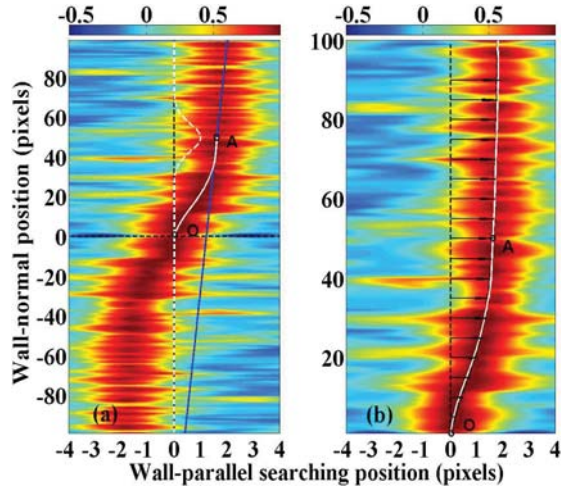


Figure 3: Velocity interpolation method applied to synthetic image templates. (a) Instantaneous normalized correlation stack (top half) combined with its 180° rotated copy. Velocity gradient measurement at a point $n = 50$ pixels, Gaussian weighted (white dash curve), line fitting (solid black line). (b) Extracted IPIV velocity profile (solid white curve) compared with PID displacement vectors (black vectors), and the true DNS profile (black dashed curve).

and r.m.s of $(I'_{m,n} - \bar{I}'_n)$ could be used with care to increase the signal-to-noise ratio in the correlation stack. Image subpixel interpolation is applied before correlation to reduce peak-locking error. Fig. 2e is an example of a normalized correlation stack $C_{U,n}$, with tangential displacement U (horizontal axis) and wall-normal position (vertical axis), obtained from a pair of image templates (c), (d) of transformed images (a), (b) with subpixel interpolation equivalent to 0.1 pixels.

Measuring wall shear and integrating velocity profile

In Nguyen and Wells (2006), the near-wall tangential velocity profile was returned by Gaussian or spline fitting to the strong peaks' positions identified from correlation stack. Such a procedure, however, was sensitive to the peak identification. One of the sources of errors was caused by a bias to the false but strong peaks instead of correct but weak ones. Besides, extrapolation and interpolation schemes were required to obtain velocity vectors at all wall-normal positions.

Our present study introduces a new method of precisely extracting velocity profiles from correlation stack by integrating measured velocity gradients $grad(n)$ upward from the wall one pixel at a time. Assuming a no-slip wall, $u(0) = 0$, this translates to:

$$u(n) = u(n - 1) + grad(n) \quad (3)$$

At position n ($n = 0, 1, \dots, N$), velocity gradient $grad(n)$ is extracted by fitting a straight line to the correlation stack, along which the Gaussian-weighted sum of correlation values in equ. 4 is maximal.

$$F(grad) \equiv \frac{\sum_{y=-N}^N C_{U,y} \Omega(y)}{\sum_{y=-N}^N \Omega(y)} \quad (4)$$

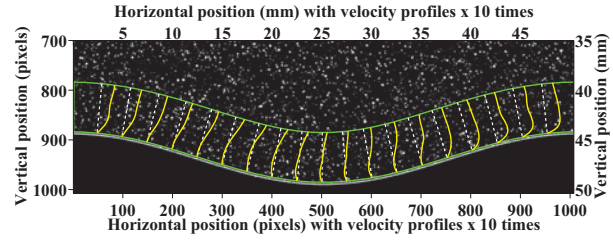


Figure 4: Detected tangential profiles $\times 10$ times by IPIV processing on synthetic image.

where

$$U(grad, y) = u(n) + (y - n)grad \quad (5)$$

The Gaussian-weighting function Ω , shown in equ. 6, is centered at the current position n .

$$\Omega(y) = \exp\left[-\frac{(y - n)^2}{2\sigma^2}\right] \quad (6)$$

Near the wall, the fitting line includes the values from a rotated copy of the correlation stack around the wall location to impose the no-slip condition.

Fig. 3a shows a velocity gradient measurement at $n = 50$ pixels with a Gaussian weighting distribution of $\sigma = 7.07$ pixels (white dash curve). The correlation stack (top half) is combined with its reflected image (bottom half). Correlation values along the straight line (blue) rotating around the point A are accumulated with Gaussian weighting function Ω . The slope of line corresponding to the maximum correlation summation is the measured velocity gradient. Compared to PIV/IG+, wall shear measurement is no longer separated from determination of the velocity profile; rather it is simply the first step in our integration process with point O fixed to enforce no-slip at the wall. As seen in fig. 3b, IPIV measurement with Gaussian $\sigma = 7.07$ yields a plausible profile (white curve) that is very close to the true profile (black dashed) based on DNS.

Reverse transforming to obtain physical values

Reverse transformation is required to obtain physical values of velocity profile and wall shear gradient. In the present version of IPIV, only wall tangential displacement component U is measured in the transformed domain. With the coordinate transformation coefficients g_ξ, g_η defined by:

$$g_\xi = \sqrt{\left(\frac{\partial x}{\partial \xi}\right)^2 + \left(\frac{\partial y}{\partial \xi}\right)^2} \quad (7)$$

$$g_\eta = \sqrt{\left(\frac{\partial x}{\partial \eta}\right)^2 + \left(\frac{\partial y}{\partial \eta}\right)^2} \quad (8)$$

the magnitude of local tangential displacement component \tilde{u} and wall shear gradient $\frac{\partial \tilde{u}}{\partial \bar{y}}$ in local coordinates (\bar{x}, \bar{y}) aligned with the wall boundary can be obtained as:

$$\tilde{u} = U g_\xi = U \sqrt{\left(\frac{\partial x}{\partial \xi}\right)^2 + \left(\frac{\partial y}{\partial \xi}\right)^2} \quad (9)$$

$$\frac{\partial \tilde{u}}{\partial \bar{y}} = \frac{\partial U}{\partial \eta} \frac{g_\xi}{g_\eta} \quad (10)$$

where $\frac{\partial U}{\partial \eta}$ is wall shear gradient measured by IPIV in the transformed image. Fig. 4 shows tangential velocity profiles produced by IPIV, overplotted on a near-wall region

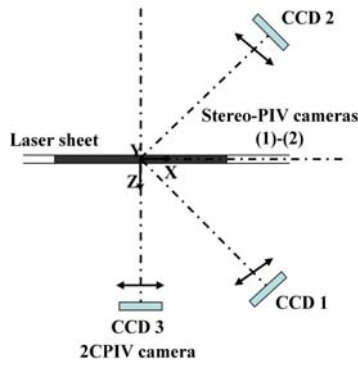


Figure 5: Camera projections for generating synthetic images.

of 1008×300 pixels synthetic image. In this example, flow separation and reattachment can be clearly observed within a template height of 100 pixels. As the friction Re , based on wave amplitude, of the DNS snapshot used to generate synthetic images is 106, the above height of 100 pixels is equivalent to about 100 wall units.

WALL SHEAR AND VELOCITY MEASUREMENTS BY IPIV AND PID TO SYNTHETIC IMAGES

To evaluate the capability of IPIV, synthetic images are generated from a DNS snapshot of turbulent flow over wavy boundaries (Nakayama and Sakio (2002); Yokojima (2002)). The DNS computational domain consists of three wavelengths and $192 \times 128 \times 96$ grid lines along the streamwise, spanwise and vertical directions. The ratio of the wave amplitude to the wave length is 0.05 with a maximum slope of 0.31. The bulk Reynolds number Re_H defined by the average velocity U_m and the flow depth H is 6760. The Reynolds number based on friction velocity and peak-to-peak height is 106. Forty pairs of 1008×1008 pixel images are synthetically projected from a field of view of $H \times H$, where $H = 50$ mm of the central wavelength as a 2CPIV (perpendicular view) and a Stereo PIV (angular view) cameras. Camera projections are sketched in fig. 5. In the synthetic image generator, the particle pattern and camera projection models proposed by Lecordier and Westerweel (2003) are implemented. Moreover, non-uniform diameter tracers are randomly scattered into a virtual 3D volume of a laser sheet. The laser sheet has a Gaussian intensity profile with $\sigma = 0.5$ mm, or about 10 wall units. Tracer image diameter has a Gaussian distribution with $\sigma = 1.28$ pixels, mean value of 2.8 pixels, and varies from 2.2 to 6 pixels. Seeding density in the resulting images is about 0.01 particle/pixel. The time delay $\Delta t = 1$ ms yields maximal tracer displacements of about 4.75 pixels.

PID and IPIV have been applied to the rectangular images, which are conformally transformed by step 2. Corresponding results of wall shear gradient and velocity profile are compared with the true values of DNS to express the accuracy of such processing techniques.

Grid spacing of PID performed to the transformed images is 5 pixels in vertical direction and about 25 pixels in horizontal direction. The first grid points are vertically located 5 pixels above the wall. The interrogation window size is 50×11 pixels with 50% overlap between horizontally and vertically adjacent windows. To attain PID convergence, the template height is reduced to 8 pixels at the wall to handle the smaller tracer displacements there. Besides, a Gaussian-smoothing scheme analogous to step 4 is

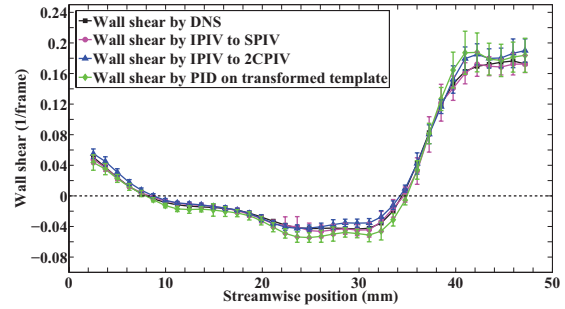


Figure 6: Wall shear measurements by IPIV (with circle and without triangle) stereo reconstruction) to 2D and 3D synthetic images compared to those of PID (diamond), and DNS data (square). Half-height of error bar corresponds to standard deviation of measured values at each position.

applied along horizontal and vertical directions to suppress the instability of PID iterations. PID wall gradients are then resulted by dividing the obtained near-wall velocities by their distances towards the wall. On the contrary, IPIV wall gradients are extracted directly from the correlation stacks.

Fig. 6 shows the sample-averaged of wall gradients obtained by PID and IPIV benchmarked with true values of DNS. Wall shear measurement by IPIV to Stereo PIV synthetic images (circles) with stereo reconstruction procedure (equ. 1) shows a better overall agreement to the DNS values (squares) rather than those by IPIV (triangles) and PID (diamonds) to 2CPIV image pairs. The r.m.s values of the gradient difference between DNS data and the sample averages of PID, IPIV to 2CPIV and IPIV to Stereo PIV images are 8.9×10^{-3} ($frame^{-1}$), 6.5×10^{-3} ($frame^{-1}$) and 3.1×10^{-3} ($frame^{-1}$) respectively.

Returning to fig. 3b, it is seen that IPIV provided a continuous profile (white curve) whereas PID displacement vectors were obtained at 5 pixel intervals in wall-normal direction. Visually, near the wall ($n \leq 30$ pixels) IPIV profile is closer to the true values of DNS data than PID. Note that the optimal conditions are implemented for both PID and IPIV processing, i.e the template height of PID is 8 pixels and the Gaussian STD σ of IPIV is 7 pixels. The same template width and horizontal search size for both PID and IPIV are 50 pixels and 8 pixels respectively. Fig. 7 shows a point-to-point comparison of near-wall tangential displacements, symbolized as $\overline{u(n)^j}$ in equ. 11, obtained by PID and IPIV on transformed images, within 15 pixels from wall. These are ensemble-averaged from 40 image pairs ($P = 40$), where j indexes the measured streamwise stations ($Q = 37$). PID data are measured at 5 pixel intervals in vertical direction, and are thus sparser than those of IPIV.

$$\overline{u(n)^j} = \frac{1}{P} \sum_{i=1}^P u(n)_i^j \quad (11)$$

Two measurement errors, random error ϵ_{rand} and total error ϵ_{total} are calculated from PID and IPIV obtained data. Random error ϵ_{rand} is defined as the r.m.s of the differences between $u(n)_i^j$ and its ensemble average $\overline{u(n)^j}$, as shown in equ. 12. Total error ϵ_{total} is defined as the r.m.s of the differences between $u(n)_i^j$ and the true profile $U(n)^j$ of DNS

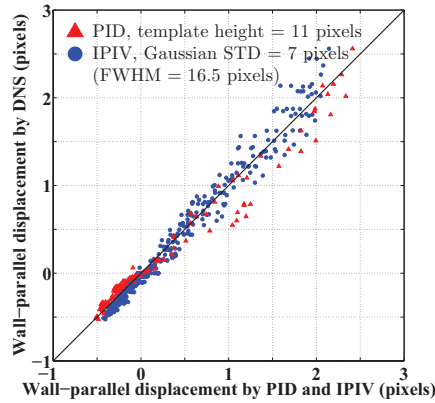


Figure 7: Comparisons of displacement measured in transformed image by IPIV (circle) and PID (triangle) against those by DNS. The straight line indicate zero error.

as expressed in equ. 13.

$$\epsilon_{rand} = \sqrt{\frac{1}{NPQ} \sum_{n=1}^N \sum_{j=1}^Q \sum_{i=1}^P (u(n)_i^j - \overline{u(n)}^j)^2} \quad (12)$$

$$\epsilon_{total} = \sqrt{\frac{1}{NPQ} \sum_{n=1}^N \sum_{j=1}^Q \sum_{i=1}^P (u(n)_i^j - U(n)^j)^2} \quad (13)$$

Fig. 7 shows that PID measurement (triangles) has more deviation from the true values than that of IPIV. As a result, its random and total errors as $(\epsilon_{rand}, \epsilon_{total}) = (0.0705, 0.1784)$ pixels are greater than those of IPIV as $(\epsilon_{rand}, \epsilon_{total}) = (0.0468, 0.1139)$ pixels. These imply that in the wall layer, our IPIV algorithm of velocity integration based on 1D correlation stack can produce more accurate measurements than vector displacements from 2D PIV correlation maps.

FLUME TEST; STEREO PIV OF BACKWARD-FACING STEP

As a practical application of IPIV to real images, an experiment was performed in an open water channel with a BFS. Channel width and step height h were 50 cm and 8.0 mm respectively. Reynolds number Re_h , based on the mean streamwise velocity U_0 and step height h , was about 2200. The water flow was seeded by hollow glass sphere particles with a mean diameter of 10 μm . The coordinate origin was situated at the step corner, with the streamwise, vertical and spanwise directions denoted by x, y and z respectively. Measurements with both two-component (2C) and three-component Stereo PIV were carried out. Measured positions are sketched in fig. 8. The fluid region in xy plane with x/h ranging from 0 to 6 was imaged using a Pulnix TM6710 CCD camera with a resolution of 640×480 pixels to form a 2CPIV system. A Stereo PIV system was established by two Kodak ES1.0 CCD cameras with a resolution of 1008×1008 pixels. Stereo PIV recorded the particle images from x/h from 0 to 7. A double pulsed Nd:YAG laser was used to illuminate a 2 mm thick vertical sheet of flow in the mid-plane of the test section. In Stereo PIV arrangement, viewing angle of cameras was set at 45° on either side of the channel from the downstream direction. The camera bodies were slightly rotated to satisfy the Scheimpflug condition. Acquisition software was adapted in LabView platform to control a PCI

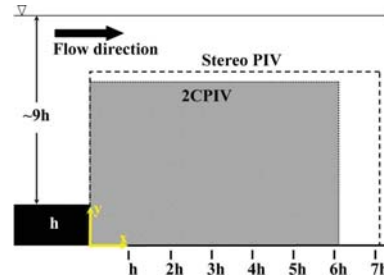


Figure 8: Measurement regions of backward-facing step experiment.

timer card for triggering laser pulses and feeding signals.

Turbulent profiles from 2CPIV and Stereo PIV

The physical dimensions of interrogation windows were 2×2 mm², 25×25 pixels for 2CPIV and 37×37 pixels for Stereo PIV. The overlap was 50% and 75% for 2CPIV and Stereo PIV respectively. The seeding density was about eight to ten particles per interrogation area. In the velocity vector computation, velocity peaks conflicting with a local median criterion were replaced by the second peak in correlation maps. Experimental images with xy plane above the level of $y/h = 0.06$ were processed by standard PIV cross-correlation algorithm.

The mean velocity and turbulent kinetic energy distributions at each streamwise location were calculated from 550 vector fields. However, with a sampling rate of 15 Hz, this quantity of velocity fields might not be sufficient to gain the flow statistics. In fig. 9a, the ensemble-averaging 2CPIV velocity profiles agreed well to those obtained by Stereo PIV. The turbulent kinetic energy profiles of Stereo PIV were calculated from u and v components. Comparison in fig. 9b shows an overall agreement of turbulent kinetic energy of 2CPIV and Stereo PIV, though a small difference at $x/h = 6$ is noted.

To acquire the wall shear, IPIV was applied to the set of 2CPIV and Stereo PIV experimental images. Wall gradient measurement was performed at an interval of 0.25 h along streamwise direction, ranging from h to 5.5 h for 2CPIV and to 6.5 h for Stereo PIV. As formulated by equ. 1, wall shears of Stereo PIV required the stereo reconstruction of wall gradients separately extracted from each view. The superscript (i) denotes wall gradients from IPIV applied to the instantaneous line correlation stack of 2CPIV and Stereo PIV images. In fig. 9c, the ensemble-averaged wall shears of 2CPIV and Stereo PIV are plotted in the same axes. A discrepancy between these profiles is noted. Half-height of error bars show the standard deviation of measured wall shears at each location. A practicable misalignment between the 2CPIV and Stereo PIV measurement planes might cause a non-overlap region projected to these cameras. Moreover, with angular viewing directions, Stereo PIV encounters the spanwise tracer displacements through the laser sheet. As a result, the measured Stereo PIV wall shears oscillate with greater deviation than the 2CPIV values.

In addition, IPIV was applied to the line correlation stacks that were ensemble-averaged (Meinhart et al. 2000) from those of 2CPIV and Stereo PIV. The obtained wall gradients were noted by superscript (a). These values are overplotted in fig. 9c with a reversed vertical axis, in this case, a good matching can be seen between 2CPIV and Stereo PIV.

For 2CPIV and Stereo PIV, the inconsistency between

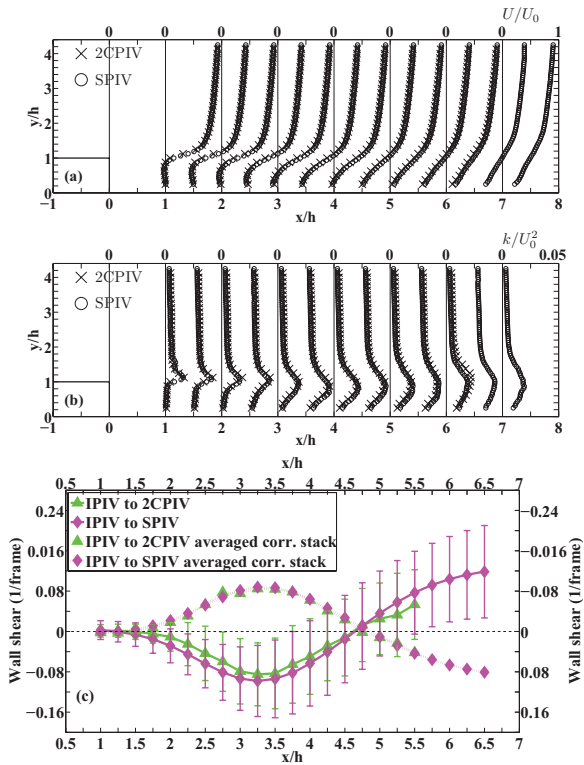


Figure 9: Backward-facing step experimental results by 2CPIV and Stereo PIV, (a) Mean streamwise velocity, (b) Turbulent kinetic energy (u and v components), (c) Wall gradients by IPIV to 2CPIV (dashed triangles) and Stereo PIV (dashed diamonds) versus wall gradients (*reversed vertical axis*) by IPIV to averaged correlation stacks of 2CPIV (dotted triangles) and Stereo PIV (dotted diamonds). Half-height of error bar corresponds to standard deviation of measured values at each position.

the gradient measurement⁽ⁱ⁾ and gradient measurement^(a) is expressed by the r.m.s values of their differences (*c.f* equ. 14). In equ. 14, $\frac{\partial U}{\partial Y}$ stands for the measured wall gradient, and K is the number of streamwise stations, $K = 19$ for 2CPIV and $K = 23$ for Stereo PIV. The resulted error from Stereo PIV as $\epsilon_{SPIV} = 0.0203$ ($frame^{-1}$) is greater than that of 2CPIV as $\epsilon_{2CPIV} = 0.0098$ ($frame^{-1}$).

$$\epsilon = \sqrt{\frac{1}{K} \sum_{k=1}^K \left(\frac{\partial U^{(i)}}{\partial Y_k} - \frac{\partial U^{(a)}}{\partial Y_k} \right)^2} \quad (14)$$

From these curves, the mean reattachment length was defined as a streamwise location where the wall gradient comes to zero. The obtained mean reattachment length $X_r = 4.62h$ for 2CPIV is very close to $X_r = 4.63h$ for Stereo PIV. In case of wall shear measured by vector differentiation, the wall-normal resolution of measurement Δy is defined as the ratio of the distance from vector location towards the wall over the step height h . For IPIV, the wall-normal resolution Δy can be considered as the ratio between the Gaussian-weighted width σ and the step height h , about $\Delta y = 0.06h$ to $0.08h$. Magnification factor and seeding density at near-wall region need to be cared if one likes to obtain higher resolution. If concerned with the accuracy of measurement, this is a considerable advantage of IPIV in comparing with standard PIV technique in the very near wall region.

CONCLUSIONS

This paper has introduced Interfacial PIV as a near-wall measurement technique. It enables to deal with curved boundaries based on conformal transformation to stretch a curved image into rectangle. A novel 1D correlation is then performed to each pixel line of transformed image templates to get a correlation stack. Our algorithm of wall-normal integrating the measured velocity gradient extracts the wall shear and a tangential velocity profile from the correlation stack. Validation with synthetic images generated from a DNS snapshot of turbulent flow over a sinusoidal bed is conducted. In our test case, IPIV yielded superior results mainly in a rather thin wall layer where the condition on wall-normal tracer displacement is satisfied. As a result, IPIV measurement of wall gradient and tangential velocity had a better accuracy comparing to PID measurement when benchmarked with DNS data. Besides, the utilization of IPIV to Stereo PIV images is confirmed by using a stereo reconstruction procedure. To examine IPIV to practical issues, experiments in an open channel with a BFS were carried out. IPIV is applied to a set of 2CPIV and Stereo PIV experimental images to draw out wall gradients. From this graph, the mean reattachment length then could be derived with a high wall normal resolution.

REFERENCES

Hochareon MB, Fontaine A, 2004, Wall shear-rate estimation within the 50cc Penn State artificial heart using PIV, *J. of Biomech. Eng.* 126, p.430-437.
 Huang HT, Fiedler HE, Wang JJ, 1993, Limitation and Improvement of PIV, *Exp Fluids* 15, p.263-273
 Ives DD, Zacharias RM, 1987, Conformal mapping and orthogonal grid generation. *AIAA/SAE/ASME/ASEE 23rd Joint Propulsion Conf.*, No. 87-2057, San Diego, California.
 Lecordier B., Westerweel J., 2003, The EUROPIV synthetic image generator (S.I.G.). In: *Particle image velocimetry: recent improvements. Proc. of the EUROPIV 2 workshop held in Zaragoza, Spain.*
 Meinhart C.D., Wereley S.T., Santiago J.G., 2000, A PIV algorithm for estimating time-averaged velocity fields, *J. of Fluids Engineering*, Vol. 122, p.285-289.
 Marr D, Hildreth E, 1980, Theory of Edge Detection, In: *Proc. of the Royal Society of London, Series B, Biological Sciences* 2007, p.187-217.
 Nakayama, A., Sakio, K., 2002, Simulation of flows over wavy rough boundaries, Center for Turbulent Research, *Annual Research Briefs*, p.313-324.
 Nguyen, C.V., Wells, J.C., 2004, Direct measurement of fluid velocity gradients at a wall by PIV image processing with Stereo Reconstruction, *J. of Flow Visualization*, V0045, p.05-027.
 Nguyen, C.V., Wells, J.C., 2006, Development of PIV/Interface Gradiometry to handle low tracer density and curved walls, FEDSM2006-98568. In *Proc. of FEDSM2006 Fluids Eng. Summer Meeting Div.*, July, Miami, USA.
 Nguyen, C.V., Nguyen, T.D., Wells, J.C., 2006b, Sensitivity of PIV/Interface Gradiometry to estimated wall position, *J. of Visualization Society of Japan* 26(2), p.203-206.
 Nguyen, C.V., Nguyen, T.D., Wells, J.C., Nakayama, A., 2008, Interfacial PIV: Velocity interpolation near curved walls, *Proc. of Int. Symp. on App. of Laser Tech. to Fluid Mech.*, 14th, Lisbon, Portugal.
 Yokojima, S., 2002, Modeling and Simulation of Turbulent Open-channel Flows Emphasizing Free-surface Effects, PhD thesis, Kobe University, Kobe, Japan.